Biogeosciences Discuss.,
https://doi.org/10.5194/bg-2019-315-AC2, 2020
© Author(s) 2020. This work is distributed under
the Creative Commons Attribution 4.0 License.

Biogeosciences
Discussions

Interactive comment on "Formation and origin of Fe-Si oxyhydroxide deposits at the ultra-slow spreading Southwest Indian Ridge" *by* Kaiwen Ta et al.

Kaiwen Ta et al.

takaiwen@sidsse.ac.cn

Received and published: 3 March 2020

Response to Reviewer

All of us would like to thank the editor and reviewer again for your considerations about this manuscript and constructive comments. We have revised it very carefully. Responses are provided in a point-by-point fashion.

Interactive comment on "Formation and origin of Fe-Si oxyhydroxide deposits at the ultra-slow spreading Southwest Indian Ridge" by Kaiwen Ta et al. Anonymous Referee #2 Received and published: 12 February 2020

RC2: The paper "Formation and origin of Fe-Si oxyhydroxide deposits at the ultra-slow spreading Southwest Indian Ridge" by Ta et al. is a geochemical study of six Fe and Si rich samples from the SWIR, collected by various means between 2008 and 2015. Although the data appears well collected and analytical work is extensive and appears sound, the context of the paper, including the introduction, interpretation of results and discussion is jumbled, and there needs to be more discussion reconciling the different analytical results.

Answer: Thanks for the reviewer's constructive comments. In the revised version, we have rewritten the manuscript to enhance readability based on your suggestion. We have made considerable efforts to reconcile the different analytical results.

RC2: For example, the low sulfur content (line 436) is inconsistent with the presence of pyrite as a major mineral (line 286).

Answer: Sorry for this mistake about the pyrite by XRD. We agree with the reviewer that the low sulfur content is inconsistent with the presence of pyrite as a major mineral. We have carefully reanalyzed XRD data. We think that pyrite is not determined in the hydrothermal Fe-Si oxyhydroxide deposits by XRD. We have corrected them in the revised paper.

RC2: also none of these major minerals (line 286) represent phyllosilicates, stated as the most abundant Fe pool obtained by the leach procedure (line 340).

Answer: Thanks for the reviewer's constructive comments. We have carefully reanalyzed XRD data. Nontronite characterized by appearance peaks at d = 3.70 Å, 3.04 and 2.16 Å, was the principal phyllosilicates observed in the spectra of sample 34II-T22.

RC2: Also, the Mössbauer shows exclusively Fe(III), however XRD reveals pyrite, Fe(II). The authors claim goethite and hematite are mineral phases (line 337-338), but do not see these via XRD, The paper does not address the possible reasons for these inconsistencies, and must.

Answer: Sorry for this mistake about the pyrite by XRD, and so at this point we have carefully reanalyzed XRD data. We think that pyrite is not determined in the hydrothermal Fe-Si oxyhydroxide deposits by XRD. We appreciate reviewer for reminding us on the discussion. We have revised the manuscript to be more clear on the XRD results as following:

The XRD results showed that 2-line ferrihydrite, hematite, nontronite, opal and birnessite composed the major minerals in the samples (Fig. S2). In the spectra of samples 21V-T7, 21V-T1 and 20V-T8, a broad peak centered at 4.08 Å suggested the presence of opal. The spectral peaks appeared at 2.69 Å and 1.60 Å in samples DIV95-1, DIV95-2, 21V-T7, 21V-T1 and 20V-T8 indicated the presence of hematite. The spectral signature of birnessite was most clearly observed in sample DIV95-2, at d = 7.06 and 2.45 Å. A small amount of birnessite was observed in DIV95-1, which was presumed to be from the residual black layer. Poorly crystalline two-line ferrihydrite, characterized by the appearance of peaks at d = 2.62 Å and 1.51 Å, was the principal mineral observed in the spectra of samples DIV95-2 and 34II-T22. Nontronite was also present in 34II-T22 deposit. In addition, halite was observed in our samples, which presumably was formed by evaporation.

RC2: The discussion is also internally inconsistent. For example, regarding the role of microbial activity in forming the Fe-Si minerals line 582 suggests “these findings support the hypothesis that microbial activity was the principal deposition mechanism of Fe-Si oxyhydroxides in modern and ancient seafloor hydrothermal systems” while line 494 notes microbes “were widely involved” and line 442 suggests that they “may have played a role.”

Answer: Thanks for the reviewer’s constructive comments. We have moderated them in the revised paper.

RC2: The conclusions (line 584-585) and line 567-569 attempt to tie in the “origin and evolution of life” which isn’t discussed in the rest of the paper and seems to be a non

sequitur to the rest of the manuscript.

Answer: We agree with this comment. We have deleted this speculative conclusions in the revised paper.

RC2: Additionally, the paper should be proofread for grammatical issues and other issues, for instance there is no "Mid Pacific Ridge", the scale bars in Figure 8 are really not visible.

Answer: Thanks for the reviewer’s constructive comments. In the revised version, We have made considerable efforts to improve the grammar and other issues of manuscript. We have delete "Mid Pacific Ridge". We have corrected the scale bars in Figure 9.

Please also note the supplement to this comment:
https://www.biogeosciences-discuss.net/bg-2019-315/bg-2019-315-AC2-supplement.pdf

---

Interactive comment on Biogeosciences Discuss., https://doi.org/10.5194/bg-2019-315, 2019.

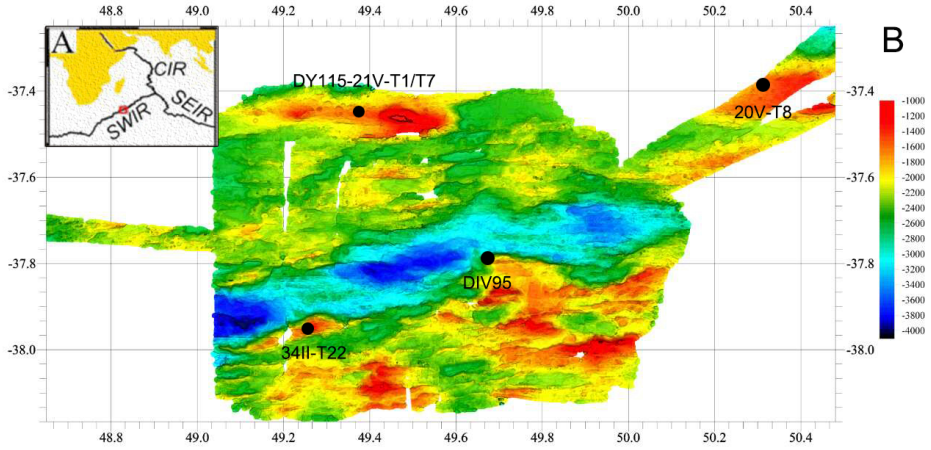

Fig. 1. Regional bathymetric map and location of the sampling site at the SWIR. Black dots represent sample locations in this study.

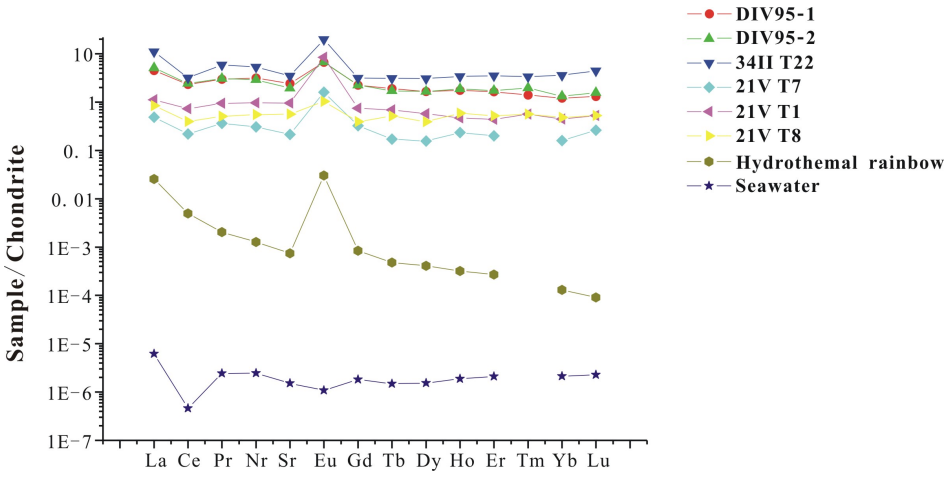

Fig. 2. Chondrite-normalized REE distribution patterns of the hydrothermal Fe-Si oxyhydroxide deposits in this study.

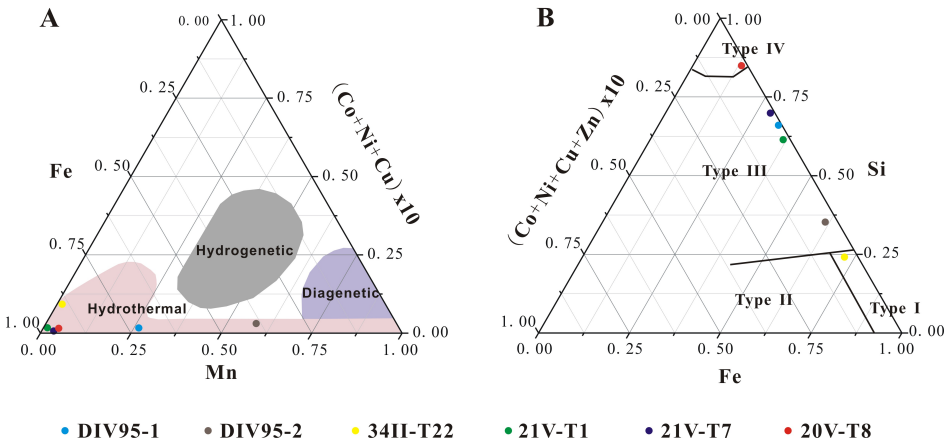

Fig. 3. (a) Ternary diagram for Mn-Fe-(Co + Ni + Cu) ×10 of Fe-Si oxyhydroxide deposits. The hydrothermal, diagenetic and hydrogenous fields were classified by Hein et al. (1994). The Fe-Si oxyhydroxide depos

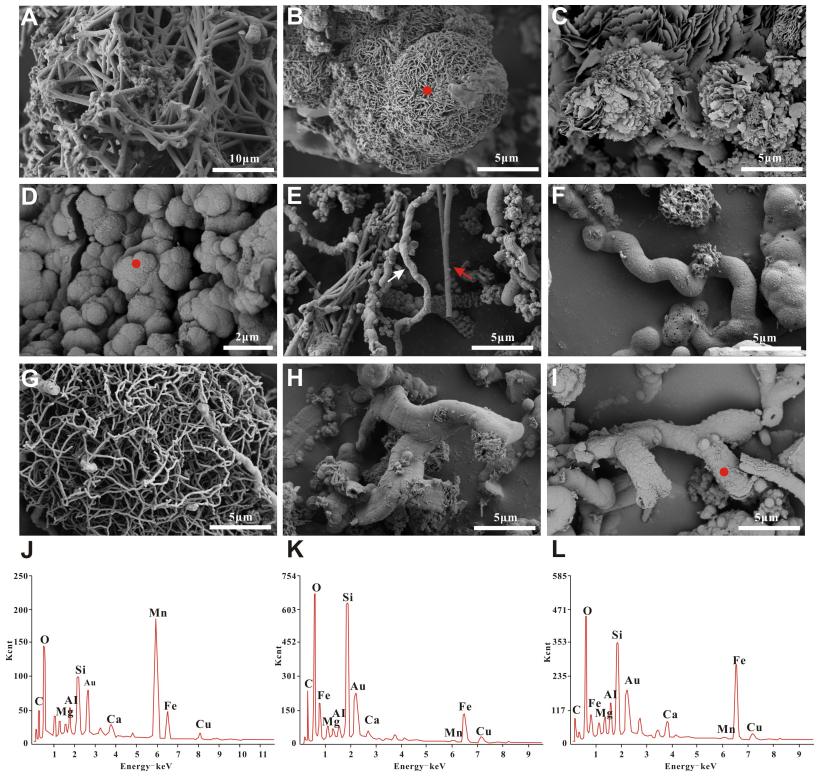

Fig. 4. SEM images showing different styles of biogenic mineral structures in different Fe-Si oxyhydroxide deposits. (a) A network-like structure composed of rod-like mineralized forms observed in the orange-

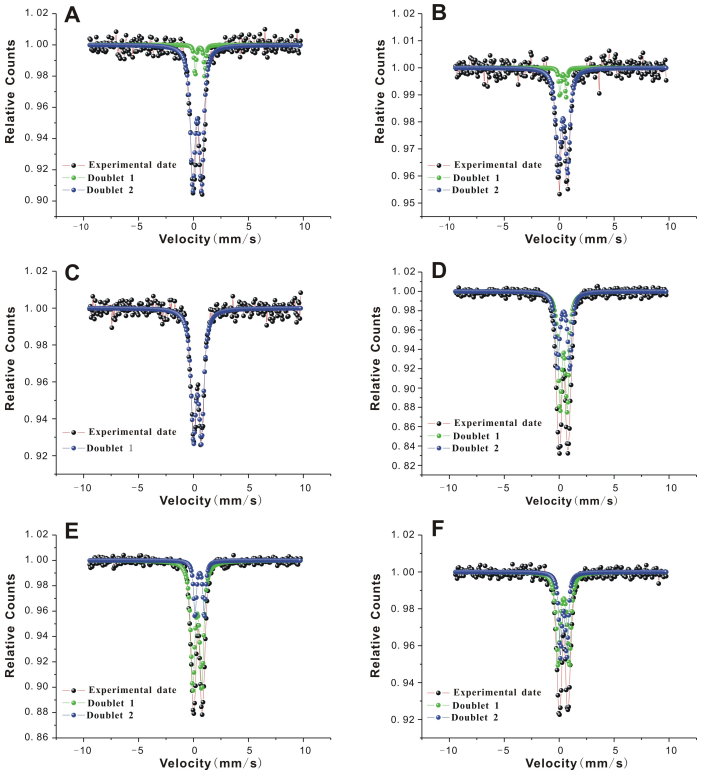

Fig. 5. 57Fe Mössbauer spectra at room temperature (300 K), and fitting results of Fe-Si oxyhydroxide deposits from the SWIR. (a) DIV95-1, (b) DIV95-2, (c) 34II-T22, (d) 21V-T1, (e) 21V-T7, (f) 20V-T8.

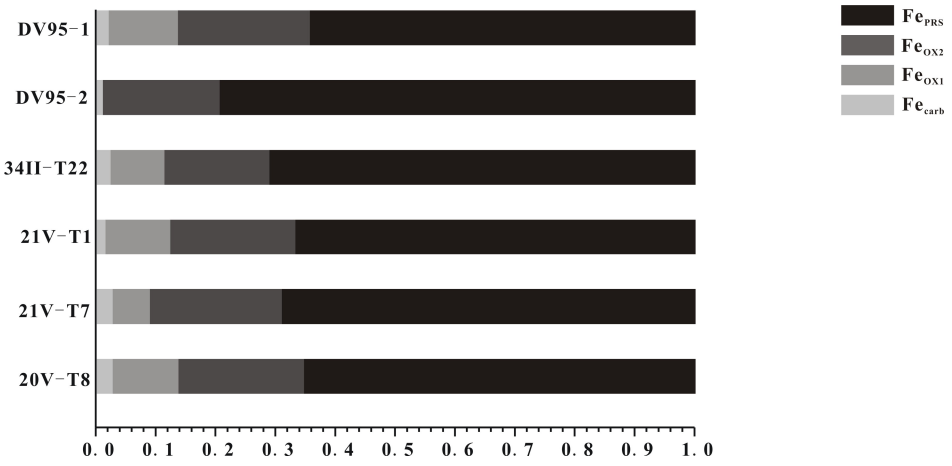

Fig. 6. Sequential extraction of iron minerals in the studied Fe-Si oxyhydroxide deposits.

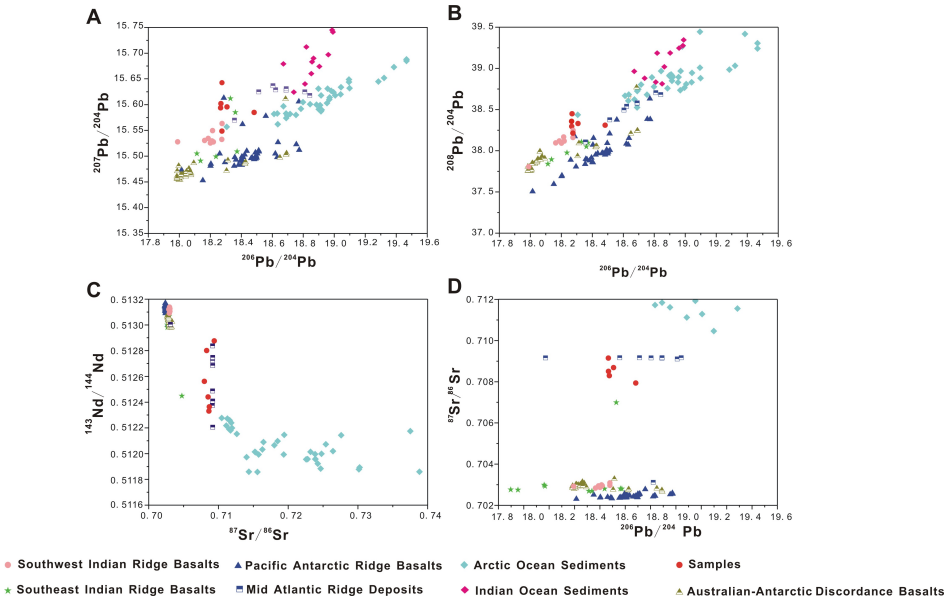

Fig. 7. Comparison of 208Pb/204Pb versus 206Pb/204Pb (a), 207Pb/204Pb versus 206Pb/204Pb (b), 87Sr/86Sr versus 143Nd/144Nd (c), and 87Sr/86Sr versus 206Pb/204Pb from the studied deposits, compared against Pac

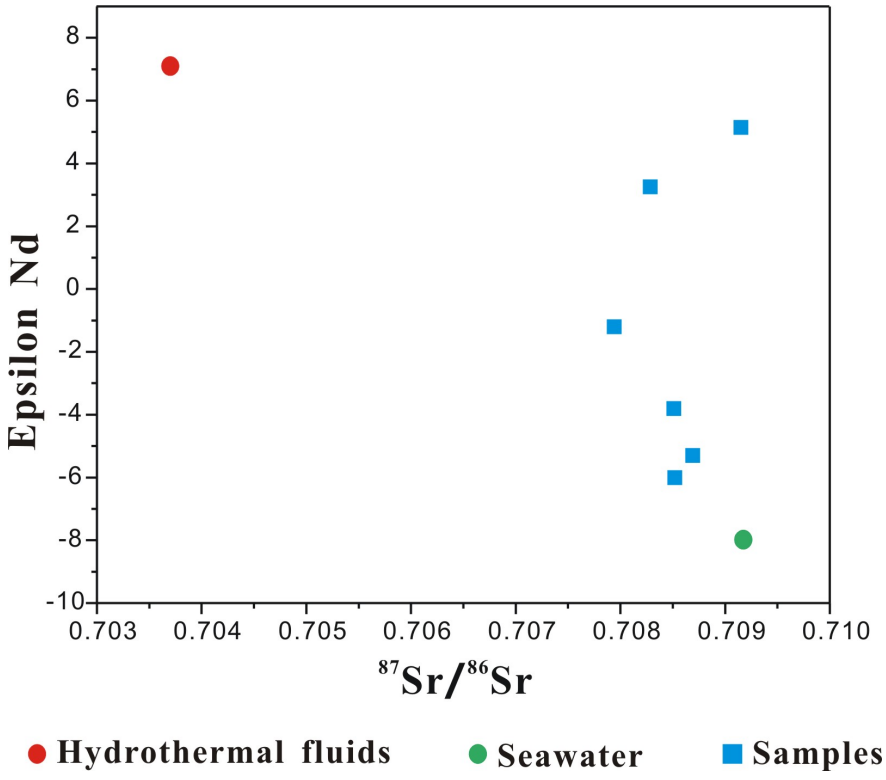

Fig. 8. Epsilon Nd versus 87Sr/86Sr for Fe-Si oxyhydroxides compared to hydrothermal fluid and seawater. Isotopic compositions of Nd and Sr based on modern Indian Ocean seawater values (ÉŻNd = −8.0, 87Sr/86Sr

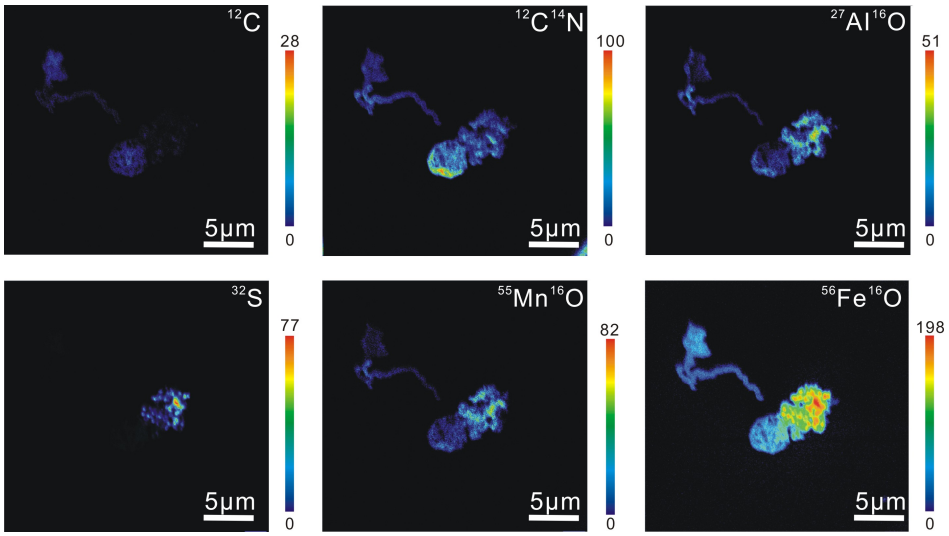

Fig. 9. NanoSIMS ionic images of 12C−, 12C14N−, 32S−, 27Al16O−, 55Mn16O−, and 56Fe16O2− from a twisted stalk. Ion intensity variations were shown by calibration bars. The scale bar was 5 μm for each panel.

Table 2. Pb, Sr, Nd,and O isotopic data for studied samples and deduced temperature.

Sample#	$^{87}Sr/^{86}Sr$	(2σ)	$^{143}Nd/^{144}Nd$	(2σ)	$^{206}Pb/^{204}Pb$	(2σ)	$^{207}Pb/^{204}Pb$	(2σ)	$^{208}Pb/^{204}Pb$	(2σ)	$^{147}Sm/^{144}Nd$	εNd	$\delta^{18}O$ (‰ SMOW)	Deduced temperture (°C)
DIV95-1	0.70851	0.000014	0.512441	0.000011	18.267	0.003	15.601	0.003	38.296	0.012	0.1416	-3.8	20.9	43.2
DIV95-2	0.70869	0.000013	0.512364	0.000011	18.307	0.003	15.595	0.003	38.331	0.009	0.1298	-5.3	/	/
34II-T22	0.70915	0.000012	0.512895	0.000015	18.266	0.002	15.594	0.002	38.357	0.006	0.1180	5.1	35.8	114.2
21V-T1	0.70852	0.000015	0.512332	0.000015	18.269	0.002	15.640	0.003	38.449	0.006	0.1645	-6	17.3	31.0
21V-T7	0.70794	0.000013	0.512578	0.000031	18.483	0.003	15.585	0.003	38.310	0.009	0.1924	-1.2	16.5	28.6
20V-T8	0.70830	0.000012	0.512801	0.000015	18.275	0.001	15.549	0.001	38.214	0.003	0.1721	3.2	20.5	41.8

Fig. 10.